

# **Superconductivity of $\text{Ca}_2\text{InN}$ with a layered structure embedding anionic indium chain array**

**Sehoon Jeong<sup>1</sup>, Satoru Matsuishi<sup>2</sup>, Kimoon Lee<sup>3</sup>, Yoshitake Toda<sup>3</sup>, Sung Wng Kim<sup>4,5</sup> and Hideo Hosono<sup>1,2,3,\*</sup>**

<sup>1</sup>Materials and Structures Laboratory, Tokyo Institute of Technology, 4259 Nagatsuta-cho, Midori-ku, Yokohama, Japan

<sup>2</sup>Materials Research Center for Element Strategy, Tokyo Institute of Technology, 4259 Nagatsuta-cho, Midori-ku, Yokohama, Japan

<sup>3</sup>Frontier Research Center, Tokyo Institute of Technology, 4259 Nagatsuta-cho, Midori-ku, Yokohama, Japan

<sup>4</sup>Department of Energy Science, Department of Physics, Sungkyunkwan University, Suwon, Korea.

<sup>5</sup>IBS Center for Integrated Nanostructure Physics, Institute for Basic Science, Sungkyunkwan University, Suwon, Korea.

E-mail: [hosono@msl.titech.ac.jp](mailto:hosono@msl.titech.ac.jp)

## Abstract

We report the emergence of superconductivity in  $\text{Ca}_2\text{InN}$  consisting of a 2-dimensional (2D) array of zigzag indium chains embedded between  $\text{Ca}_2\text{N}$  layers. A sudden drop of resistivity and a specific-heat ( $C_p$ ) jump attributed to the superconducting transition were observed at 0.6 K. The Sommerfeld coefficient  $\gamma = 4.24 \text{ mJ/mol K}^2$  and Debye temperature  $\Theta_D = 322 \text{ K}$  were determined from the  $C_p$  of the normal conducting state and the superconducting volume fraction was estimated to be  $\sim 80\%$  from the  $C_p$  jump, assuming a BCS-type weak coupling. Density functional theory calculations demonstrated that the electronic bands near the Fermi level ( $E_F$ ) are mainly derived from In  $5p$  orbitals with  $\pi$  and  $\sigma$  bonding states and the Fermi surface is composed of cylindrical parts, corresponding to the quasi-2D electronic state of the In chain array. By integrating the projected density of states of In- $p$  component up to  $E_F$ , a valence electron population of  $\sim 1.6$  electrons/In was calculated, indicating that the partially anionic state of In. The In  $3d$  binding energies observed in  $\text{Ca}_2\text{InN}$  by x-ray photoemission spectroscopy were negatively shifted from that in In metal. The superconductivity of  $\text{Ca}_2\text{InN}$  is associated with the  $p$ - $p$  bonding states of the anionic In layer.

## 1. Introduction

Superconductivity of magnesium diboride ( $\text{MgB}_2$ ) shows the highest critical temperature ( $T_c = 39$  K) among the intermetallic compounds [1]. Therefore, related intermetallic compounds have attracted attention as potential new superconductors.  $\text{MgB}_2$  is composed of a graphite-structured hexagonal boron (B) layer and a layer of magnesium (Mg) atoms. Since electrons are transferred from Mg to B, the formal charge of B is  $-1$  with electronic configuration of  $2s^2 2p^2$ . The metallic state is derived via electron transfer from the  $\sigma$  bands made up of B  $p_{x,y}$  orbitals to the  $\pi$  bands containing B  $p_z$  orbitals [2-4]. We can find similar anionic  $p$ -block metal layers in other intermetallic superconductors. For example, the anionic Bi ( $6s^2 6p^4$ ) square net produced by Bi  $6p$ -Bi  $6p$   $\sigma/\pi$  bonding is responsible for the superconductivity of  $R\text{Ni}_x\text{Bi}_2$  ( $R = \text{La, Ce, Nd}$  and Y) compounds [5]. Moreover, the superconductive Zintl phases such as  $AE\text{Sn}_x$  ( $AE = \text{Sr, Ba}$ ) have intermetallic anionic Sn-layered structures containing  $\pi$  bonding systems [6, 7].

In this paper, we report the investigation of superconductivity (critical temperature  $T_c = 0.6$  K) in  $\text{Ca}_2\text{InN}$  [8] containing a 2-dimensional (2D) chain array of anionic In ( $5s^2 5p^{1+\delta}$ ). Density functional theory (DFT) calculations and X-ray photoemission spectroscopy (XPS) measurements indicate that the superconductivity arises from the anionic state of the In layer [ $-(\text{In}^{0.6})-$ ] which is formed by In  $5p$  orbitals with  $\pi$  and  $\sigma$  bonding states.

## 2. Experimental details

The polycrystalline  $\text{Ca}_2\text{InN}$  was synthesized by the reaction of  $\text{Ca}_2\text{N}$  and In metal. All handling was performed in an argon-filled glove box with oxygen and moisture levels below 1 ppm. The starting  $\text{Ca}_2\text{N}$  powder was synthesized by solid-state reaction between  $\text{Ca}_3\text{N}_2$  powder and Ca shots as described in reference [8]. A mixture of  $\text{Ca}_2\text{N}$  and In was pressed into a pellet and the pellet was wrapped with molybdenum foil and sealed into a silica glass ampoule filled with argon gas at atmospheric pressure. The ampoule was then heated at 873 K for 50 h. For

homogeneity, the obtained samples were ground and heated again under the same conditions. Sintered  $\text{Ca}_2\text{InN}$  polycrystalline samples were tinted dark brown, and decomposed when exposed to air.

The crystalline phase and structure were identified by powder x-ray diffraction (PXRD) using  $\text{Mo K}\alpha$  radiation at 300 K. The sample was ground into a powder and placed in a glass capillary ( $\phi$  0.5 mm) to reduce effects of preferential orientation of crystallites. Rietveld refinement of the PXRD patterns was performed using TOPAS software [9].

The temperature dependence of dc electrical resistivity ( $\rho$ ) and heat-capacity ( $C_p$ ) were measured in the temperature range of 0.4-300 K both without and with a static magnetic field of up to 2 kOe, using a physical property measurement system (PPMS) with  $\text{He}^3$  refrigeration system. Electronic band structure, density of state (DOS) and Fermi surface calculations were performed using the generalized gradient approximation (GGA), Perdew-Burke-Ernzerhof (PBE) functional, and the projected augmented plane-wave (PAW) method [10, 11] implemented in the Vienna *ab initio* simulation program (VASP) code [12]. A primitive unit cell containing two chemical formula units was used, and the plane-wave basis-set cutoff was set to 900 eV. For Brillouin-zone integrations to calculate the total energy and DOS,  $8 \times 8 \times 20$  Monkhorst-pack  $k$  point grids were used [13]. To obtain the projected DOS, the charge density was decomposed over the atom-centered spherical harmonics; Wigner-Seitz radii of 0.20(1) nm for In, 0.16(8) nm for Ca and 0.08(3) nm for N were used for the PDOS calculation. The Fermi surface was visualized using Xcrysden software [14]. The electron localization function (ELF) was calculated to clarify the chemical bonding state by identifying whether the electrons were localized or delocalized.

The oxidation state of  $\text{Ca}_2\text{InN}$  was confirmed by XPS and ultraviolet photoelectron spectra (UPS) measurements using a hemispherical analyzer [x-ray ( $\text{Mg K}\alpha$  line:  $h\nu = 1253.6$  eV) source and Non-monochromatic UV photons (He I line:  $h\nu = 21.2$  eV) source]. To prepare a

clean surface, the sample was cleaved under high vacuum. All XPS spectra were measured at room temperature and displayed as a function of the electron binding energy with respect to the Fermi level. The core level spectra were subsequently deconvoluted using a least squares Gaussian fit method.

### 3. Results and discussion

All peaks in the PXRD pattern could be indexed to an orthorhombic structure (space group: Cmc<sub>2</sub>m) with lattice parameters:  $a = 0.352(9)$  nm,  $b = 2.020(7)$  nm and  $c = 0.496(9)$  nm (See figure S1 and table S1 of supplementary data). These values agreed well with those in the literature [15]. Figure 1 shows the crystal structure of Ca<sub>2</sub>InN, made up of alternate Ca<sub>2</sub>N layer and one dimensional zigzag chains of In layers along the  $b$ -axis [15]. The Ca<sub>2</sub>N layer consists of edge shared Ca<sub>6</sub>N octahedra and contains two non-equivalent Ca sites respectively shared by two and four octahedra. Each Ca<sub>2</sub>N layer has separation of 0.468 nm, which is 20 % larger than that found in Ca<sub>2</sub>N (0.386 nm) [8]. The In layer embedded between the Ca<sub>2</sub>N layers forms an array of zigzag chains parallel to the  $c$ -axis. The In-In-In bond angle is 115.12° and In-In bond length is 0.294 nm, which is 10 % shorter than the shortest separation (0.325 nm) in metallic In. The inter-chain In-In distance (along the  $a$ -axis) is 0.353 nm, which is 20 % larger than the intra-chain In-In bond length.

Figure 2(a) shows the temperature dependence of electrical resistivity. Metallic behavior, with resistivity decreasing with decreasing temperature, was seen; the resistivity value at room temperature was 27 mΩ·cm. A sudden drop to zero resistivity occurred at 0.7 K; this drop was not seen when a magnetic field of  $H = 2$  kOe [inset of figure 2(a)] was applied. Figure 2(b) shows specific heat data (plotted as  $C_p/T$  vs.  $T^2$ ), below 1.2 K, collected at  $H = 0$  and 2 kOe. A jump was observed from  $T = 0.7$  K without magnetic field, but was completely suppressed when  $H = 2$  kOe. These results clearly indicate that bulk superconductivity appears from 0.7 K. The

specific heat above  $T = 0.7$  K when  $H = 0$  Oe, i.e., in the non-superconducting state, can be fitted to the formula:

$$C_p / T = (C_e + C_l) / T = \gamma + \beta T^2 \quad (1)$$

where  $C_e$  and  $C_l$  denote electronic and lattice contributions to the total specific heat [16]. The obtained  $\gamma$  and  $\beta$  values were 4.24 mJ/mol K<sup>2</sup> and 1.39 mJ/mol K<sup>4</sup>, respectively. The inset of figure 2(b) shows the electronic specific heat data (plotted as  $C_e/T$  vs.  $T$ ) for Ca<sub>2</sub>InN.  $T_c^{\text{mid.}} = 0.6$  K was defined as the midpoint of the specific heat jump, and the height of the heat capacity jump ( $\Delta C_p^{\text{obs.}}$ ) was 2.85 mJ/mol K. The Debye temperature ( $\Theta_D$ ) is estimated as 322 K by using:

$$\Theta_D = (12\pi^4 n R / 5\beta)^{1/3} \quad (2)$$

where  $n$  is the number of atoms per formula unit of Ca<sub>2</sub>InN and  $R$  is the gas constant. To evaluate the electron-phonon coupling constant ( $\lambda_{\text{el-ph}}$ ), we use McMillan's expression[17]:

$$T_c^{\text{mid.}} = (\Theta_D / 1.45) \exp\{[-1.04(1 + \lambda_{\text{el-ph}})] / [\lambda_{\text{el-ph}} - \mu^*(1 + 0.62\lambda_{\text{el-ph}})]\} \quad (3)$$

where the  $\mu^*$  is the retarded Coulomb repulsion parameter and usually amounts to 0.1- 0.2. Substituting 0.1 and 0.2 for  $\mu^*$ , we get  $\lambda_{\text{el-ph}} = 0.36$  for 0.1 and  $\lambda_{\text{el-ph}} = 0.53$  for 0.2, and find that Ca<sub>2</sub>InN is classified as a weak-coupling BCS-type superconductor [17].

According to BCS theory for weak coupling, the superconducting volume fraction was evaluated to be 78% from

$$\Delta C_p^{\text{obs.}}(T_c) / \Delta C_p^{\text{BCS}}(T_c) \quad (4)$$

where the theoretical heat jump at  $T_c$  ( $\Delta C_p^{\text{BCS}}$ ) is predicted to 3.64 mJ/mol K from BCS theory.

$$\Delta C_p^{\text{BCS}}(T_c) / \gamma T_c = 1.43 \quad (5)$$

Figure 3(a) shows the calculated electronic band structure, with total and projected DOS

(PDOS) per formula unit (f. u.), for  $\text{Ca}_2\text{InN}$ . Here, we noted that the narrow entangled bands located from  $-3$  to  $-1$  eV with Ca  $d$  character did not appear in the band structure calculated by extended Hückel method in the past report [15]. This difference is due to a flaw of the calculation method ignoring the contribution of Ca  $3d$  orbitals. The four bands which cross the  $E_F$  and form a DOS peak around  $E_F$  ( $-0.9$  eV  $< E < 2.0$  eV) are mainly made up of In  $5p$  bands with small contributions from the atomic orbitals of Ca and N, as shown in the PDOS. The energy levels of N and Ca are far from the  $E_F$ , and In  $5p$  bands are inserted between the N  $2p$  and Ca  $3d$  bands. By integrating the PDOS on the In  $5p$  orbital up to  $E = E_F$ , we find that the valence of In in  $\text{Ca}_2\text{InN}$  is  $\text{In}^{0.6-}$ , i.e., the electronic configuration of In may be expressed as  $[\text{Kr}]4d^{10}5s^25p^{1.6}$ . This calculated result indicates that the anionic indium layer includes a  $p$ -band, which is stabilized by the strong electron donating ability of the  $[\text{Ca}_2\text{N}]^+$  cationic framework. The cationic  $\text{Ca}_2\text{N}$  layer is also found in dicalcium nitride  $\text{Ca}_2\text{N}$  regarded as 2D electride  $[\text{Ca}_2\text{N}]^+e^-$ , while the connecting pattern of  $\text{Ca}_6\text{N}$  octahedron is a little different [8, 18]. The ionicity of  $\text{Ca}_2\text{N}$  layer is so strong that electrons are pushed out to empty inter-layer space.

Figure 3(b) shows the Fermi surface of  $\text{Ca}_2\text{InN}$ . The two kinds of cylindrical sheets along  $\Gamma$ -Y, which are parallel to the direction of the alternate stacking of  $\text{Ca}_2\text{N}$  and In layers ( $b$ -direction in conventional cell), are perpendicular to the In-chain array direction ( $a$ - and  $c$ -direction in conventional cell). Additionally, one kind of the cylindrical sheets around the R and S points consist of flat planes along the  $\Gamma$ -Z direction, which are perpendicular to the In-chain direction ( $c$ -axis; figure 1). This result suggests that the embedded In zigzag chain (quasi-one-dimensional) array in  $\text{Ca}_2\text{InN}$  has an electronic structure with 2D character, with some flat areas in the Fermi surface because of the binding state within the In-chain array. The 3D character, which occurs along the  $\Gamma$ -Z direction, comes from the orbital interactions between In  $5p$  and Ca  $3d$ , N  $2p$ . The electronic structure can also be seen in the calculated ELF in figure 3(c). The large ELF values around Ca and N atoms reflect that the chemical bond between Ca

and N atoms is ionic. In contrast, the small ELF values spread around the In-chain direction and inter-chain direction indicate that the electrons are 2D delocalized along the In-chain array, and are independent from the  $\text{Ca}_2\text{N}$  layer.

Figure 3(d) shows orbital angular momentum projected DOS on In site. The In  $5p_x$ ,  $5p_y$  and  $5p_z$  orbitals contribute to the four entangled bands near  $E_F$ . These bands are dispersed along  $\Gamma$ -S, R-Z (along the  $a$ -direction) and S-R (along the  $c$ -direction). These results imply that the electronic properties of  $\text{Ca}_2\text{InN}$  are attributable to the  $p\sigma$  and  $p\pi$  bonding complex in the  $a$ -, and  $c$ -directions (In-chain array plane) of the In  $5p$  orbital, which is occupied by electrons supplied from the  $[\text{Ca}_2\text{N}]^+$  cationic layer. The In-In distance along In-chain shorter than that in In metal is consistent with the participation of  $p\sigma$  and  $p\pi$  bonding nature to the intra In-In bonding. In other words, electrons mainly occupy the bonding molecular orbitals of  $-(\text{In})_n-$  polymer and the bond length is shortened as a result. This is in contrast to the bonding state of indium metal in which each In atom is loosely bound by metallic bonding mediated by 3-dimensionally delocalized  $5s$  and  $5p$  electrons. Therefore, we identify that the superconductivity in  $\text{Ca}_2\text{InN}$  originates from the In  $5p$  state of the In-chain array. The strength of intra-chain bonding has been confirmed by means of crystal orbital overlap populations calculation in the reference [15]. Because the anionic In ( $5s^2 p^{1.6}$ ) state induces a complex  $\sigma$  and  $\pi$  bonding state, and the In structure has a low dimensionality electronic structure because of the In zigzag chain array, the In  $5p$  state in  $\text{Ca}_2\text{InN}$  has a more narrow band dispersion than that found in either the 3D cationic In  $5s$  or 3D anionic In  $5p$  states. Actually, the 2D anionic In ( $\text{In}^{0.6-}$ ) state in  $\text{Ca}_2\text{InN}$  has a narrower band width ( $\sim 4.1$  eV) than that of the 3D anionic In ( $\text{In}_5^{7-}$ ) band in  $\text{Sr}_3\text{In}_5$  zintl phase ( $\sim 5$  eV) [19].

Finally, the charge state of In was examined by XPS. Figure 4 shows the In  $3d$  XPS spectrum of the sample. Two peaks are identified as In  $3d_{3/2}$  at 451.0 eV and In  $3d_{5/2}$  at 443.5 eV. A shoulder at 444.5 eV was assigned to  $\text{In}^{3+}$ , originating from the surface state [20, 21]. These observed In  $3d$  binding energies show a significant lower energy shift compared to those of



indium oxide ( $444.5 \pm 0.1$  eV; +3 charge state) and pure indium ( $443.9 \pm 0.1$  eV; neutral state) [22-24]. This finding indicates that the charged state of In in  $\text{Ca}_2\text{InN}$  is negative, which is compatible with DFT calculations ( $\text{In}^{0.6-}$ ), and demonstrates that  $\text{Ca}_2\text{N}$  electride acts as a strong electron donor.

Since the  $\text{Ca}_2\text{InN}$  and In metal are weak coupling BCS type superconductor [25-26], the  $T_c$  can be estimated by the equation:

$$T_c = 1.13 \theta_D \exp(-1 / VN(E_F)) \quad (6)$$

where  $\theta_D$ ,  $V$  and  $N(E_F)$  are Debye temperature, the pairing potential of electron-electron interaction and the density of state at the  $E_F$ , respectively. As evidence from equation (6),  $N(E_F)$  and  $V$  are the dominant factors for  $T_c$  determination, whereas  $\theta_D$  plays a minor role. By putting experimental values of  $T_c$  and  $\theta_D$ , and the calculated value of  $N(E_F)$  by DFT to equation (6), the value of  $V$  was estimated. Table 1 summarizes the parameters associated with superconductivity of  $\text{Ca}_2\text{InN}$  and In metal. While  $V$  is close in these systems,  $\theta_D$  of  $\text{Ca}_2\text{InN}$  is 3 times higher than that of In metal, corresponding to strength of In-In bond. However,  $N(E_F)$  of  $\text{Ca}_2\text{InN}$  is 0.5 times smaller than that of In metal. This small  $N(E_F)$  is the main reason for lower  $T_c$  of  $\text{Ca}_2\text{InN}$ , though 2D structure is generally considered to be favorable to enhance  $N(E_F)$ . This result implies that  $\text{Ca}_2\text{N}$  block layer is rather thick to get the high volume density of In chain.

#### 4. Summary

We reported a BCS-type superconductivity with  $T_c = 0.6$  K in  $\text{Ca}_2\text{InN}$  composed of 2D anionic In-chain array embedded between  $\text{Ca}_2\text{N}$  layers. By assuming a BCS-type weak coupling, the superconducting volume fraction was estimated to be ~80%. From DFT calculations, we conclude that the superconductivity arises due to the anionic state of the In layer [ $-(\text{In}^{0.6-})$ ] which is formed by In  $5p$  orbitals with  $\pi$  and  $\sigma$  bonding states. The anionic state of In was experimentally confirmed by the XPS chemical shift. The strong ionicity of  $\text{Ca}_2\text{N}$  layer could be

applied for stabilizing various anionic metal layer forming  $p\sigma$  and  $p\pi$  bonding system similar to  $\text{MgB}_2$  and related compounds. If an appropriate  $p$ -block elemental is chosen and embedded instead of In, we expect that the resulting compound would also exhibits superconductivity.

### **Acknowledgments**

This work was supported by the JSPS FIRST project and the MEXT Element Strategy Initiative project.

## References

- [1] Nagamatsu J, Nakagawa N, Muranaka T, Zenitani Y, and Akimitsu J 2001 *Nature* **410** 63.
- [2] An J, and Pickett W 2001 *Phys. Rev. Lett.* **86** 4366.
- [3] Kortus J, Mazin I, Belashchenko K D, Antropov V, and Boyer L 2001 *Phys. Rev. Lett.* **86** 4656.
- [4] Vinod K, Varghese N, and Syamaprasad U 2007 *Supercond. Sci. Technol.* **20** R31.
- [5] Mizoguchi H, Matsuishi S, Hirano M, Tachibana M, Takayama-Muromachi E, Kawaji H, and Hosono H 2011 *Phys. Rev. Lett.* **106** 057002.
- [6] Fässler T F, Hoffmann S, and Kronseder C 2001 *ZAAC* **627** 2486.
- [7] Hoffmann S, and Fässler T F 2003 *Inorg. Chem.* **42** 8748.
- [8] Lee K, Kim S W, Toda Y, Matsuishi S, and Hosono H 2013 *Nature* **494** 336.
- [9] TOPAS, 2009 *Version 4.2* (Karlsruhe, Germany: Bruker AXS).
- [10] Blöchl P E 1994 *Phys. Rev. B* **50** 17953.
- [11] Perdew J P, Burke K, and Ernzerhof M 1996 *Phys. Rev. Lett.* **77** 3865.
- [12] Kresse G, and Furthmüller J 1996 *Phys. Rev. B* **54** 11169.
- [13] Monkhorst H J, and Pack J D 1976 *Phys. Rev. B* **13** 5188.
- [14] Kokalj A 2003 *Comput. Mater. Sci.* **28** 155.
- [15] Bailey M, and DiSalvo F 2003 *J. Alloys Compd.* **353** 146.
- [16] Charles P P, Horacio A F, Richard J C, and Ruslan P, 2007 *Superconductivity* (Oxford,UK: Academic Press) pp 11-14.
- [17] McMillan W 1968 *Physical Review* **167** 331.
- [18] Walsh A, and Scanlon D O 2013 *Journal of Materials Chemistry C* **1** 3525.
- [19] Seo D K, and Corbett J D 2001 *J. Am. Chem. Soc.* **123** 4512.
- [20] Faur M, Faur M, Jayne D T, Goradia M and Goradia C 1990 *Surf. Interface Anal.* **15** 641.
- [21] Himmerlich M, Wang C Y, Cimalla V, Ambacher O, and Krischok S 2012 *J. Appl. Phys.* **111** 093704.
- [22] Hollinger G, Skheyta-Kabbani R, and Gendry M 1994 *Phys. Rev. B* **49** 11159.
- [23] Wagner C D, Riggs W M, Davis L E, and Moulder J F 1979 *Handbook of x-ray photoelectron spectroscopy: a reference book of standard data for use in x-ray photoelectron spectroscopy* (Minnesota, USA: Perkin-Elmer Corp.) pp 116-117
- [24] Powell C J 2012 *J. Electron. Spectrosc. Relat. Phenom.* **185** 1.
- [25] Maksimov E G, and Motulevich G P 1972 *Sov. Phys.* **34** 219
- [26] Sven P R, Bauer R, Liu A Y, and Freericks J K 1998 *Phys. Rev. B* **58** 14511.

## Figure Captions

**Figure 1** Crystal structure of  $\text{Ca}_2\text{InN}$ . Green, light blue and gold spheres represent Ca, N and In atoms, respectively. Solid and dashed dark brown lines represent the conventional and primitive unit cell. Bond angle and distances were obtained from Rietvelt analysis.

**Figure 2** Physical properties of  $\text{Ca}_2\text{InN}$ . (a) Temperature dependence of electrical resistivity ( $\rho$ ). Inset shows  $\rho - T$  curves under magnetic fields of 0 (open circle) and 0.2 kOe (open square). (b) Low temperature heat capacity under magnetic fields of 0 (open circle) and 0.2 kOe (open square). Inset is the temperature dependence of the electronic specific heat data divided by temperature,  $C_e / T$ . The solid gray curve is the theoretical curve according to BCS theory [16].

**Figure 3** Calculated electronic structure of  $\text{Ca}_2\text{InN}$ . (a) Band structure and total density of states (DOS) and atomic projected DOS (PDOS). For the band structure, the green, blue and red circle size lines on the left-hand side of the figure denote the widths of the atomic distributions of Ca, In and N. In the DOS, the black line denotes the total DOS of  $\text{Ca}_2\text{InN}$ , and the green, blue, orange and red lines denote the Ca  $d$ , In  $p$ , In  $s$  and N  $p$ , DOS, respectively. (b) Fermi surface of the first Brillouin zone. Some of the high symmetry points are shown. (c) Electron-localization function (ELF) of the total electron density on the (2 0 0), (0 0 3) plane parallel to the  $b$ -axis. Solid dark brown lines represent the primitive unit cell. (d) PDOS of In  $5p$ . The black, pink and blue line thicknesses indicate the widths of the distributions of energy of the  $p_x$ ,  $p_y$ , and  $p_z$  components of the In  $5p$ , respectively. Beside the PDOS, a schematic of the bonding state on the zigzag In chain is shown. The gold spheres represent the In atoms.

**Figure 4** X-ray photoemission spectrum of  $\text{Ca}_2\text{InN}$  (In  $3d$  region). Solid lines (blue and red) are the results of Gaussian deconvolution of the peak. The inset shows the He I ( $h\nu = 21.2$  eV) ultraviolet photoelectron spectrum (UPS) valence band of  $\text{Ca}_2\text{InN}$ .

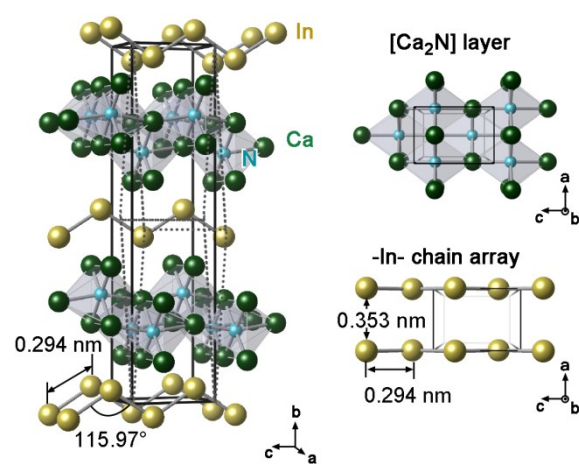


**Figure 1**

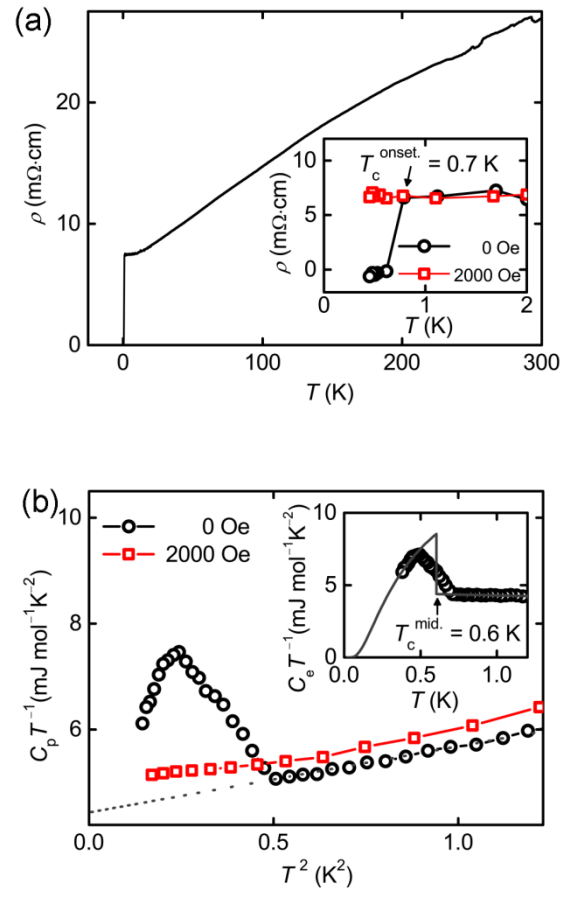


**Figure 2**

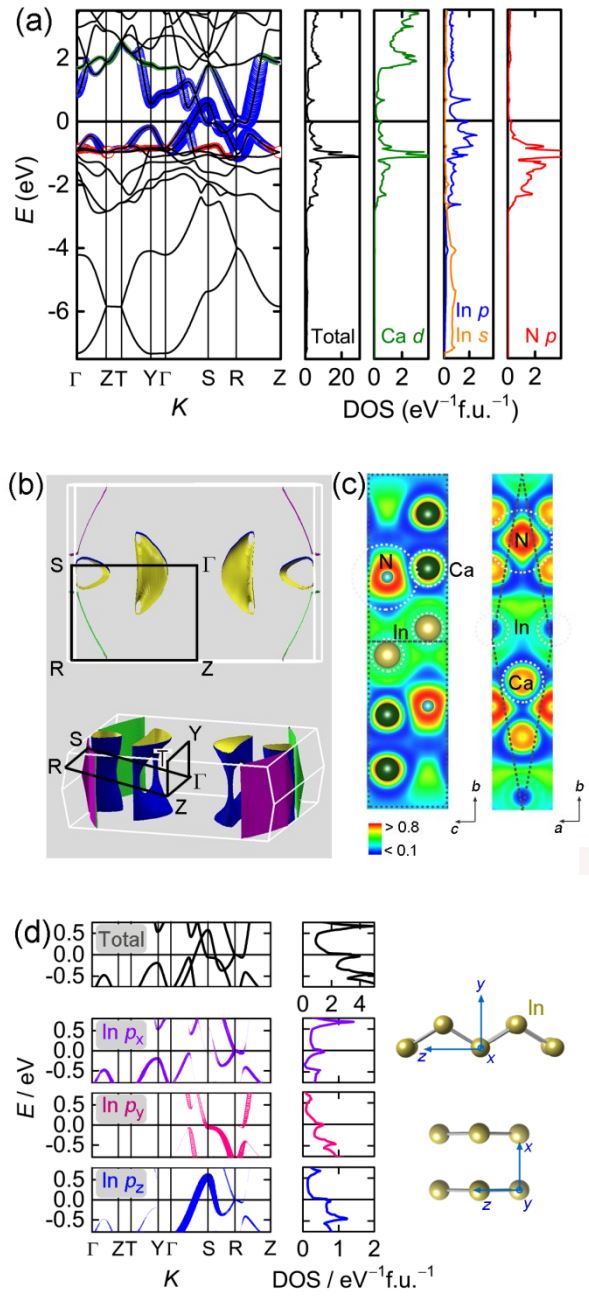


**Figure 3**

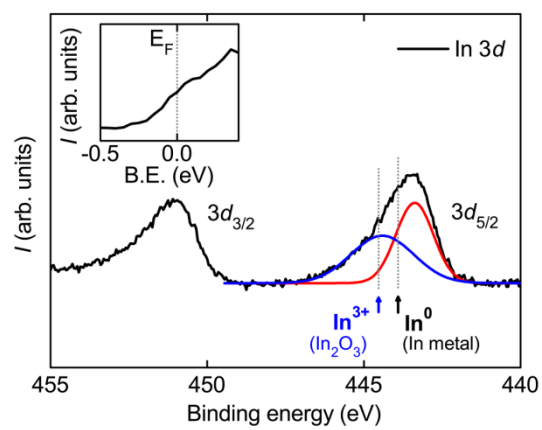


**Figure 4**



**Table 1.** Comparison of the superconducting parameters between  $\text{Ca}_2\text{InN}$  and In metal.

$\text{Ca}_2\text{InN}$	Parameter	In metal
0.6	$T_c$ (K)	3.41
322	$\Theta_D$ (K)	108
2.29	$N(E_F)$ ( $\text{eV}^{-1}\cdot\text{nm}^{-3}$ )	4.59
0.068	$V$	0.058